ChemComm

Chemical Communications

# Accepted Manuscript

This article can be cited before page numbers have been issued, to do this please use: P. F. M. Filho Marques de Oliveira, A. A.L. Michalchuk, A. G. Buzanich, R. Bienert, R. M. Torresi, P. Camargo and F. Emmerling, *Chem. Commun.*, 2020, DOI: 10.1039/D0CC03862H.




ROYAL SOCIETY OF CHEMISTRY

rsc.li/chemcomm

View Article Online
DOI: 10.1039/D0CC03862H

COMMUNICATION

# Tandem X-ray absorption spectroscopy and scattering for in situ time-resolved monitoring of gold nanoparticle mechanosynthesis

Received 00th January 20xx,
Accepted 00th January 20xx

DOI: 10.1039/x0xx00000x

Paulo F. M. de Oliveira,*[a,b] Adam A.L. Michalchuk,[b†] Ana de Oliveira Guilherme Buzanich,[b†] Ralf Bienert,[b] Roberto M. Torresi,[a] Pedro H. C. Camargo[a,c] and Franziska Emmerling*[b]

**Current time-resolved in situ approaches limit the scope of investigations possible. Here we develop a new, general approach to simultaneously follow the evolution of bulk atomic and electronic structure during a mechanochemical synthesis. This is achieved by coupling two complementary synchrotron-based X-ray methods: X-ray absorption spectroscopy (XAS) and X-ray diffraction. We apply this method to investigate the bottom-up mechanosynthesis of technologically important Au micro and nanoparticles in the presence of three different reducing agents, hydroquinone, sodium citrate, and $NaBH_4$. Moreover, we show how XAS offers new insight into the early stage generation of growth species (e.g. monomers and clusters), which lead to the subsequent formation of nanoparticles. These processes are beyond the detection capabilities of diffraction methods. This combined X-ray approach paves the way to new directions in mechanochemical research of advanced electronic materials.**

Interest in mechanochemistry has surged across the chemical sciences.[1,2] Regarded as an environmentally benign, rapid, and facile synthesis method, IUPAC dubbed mechanochemical techniques amongst the '10 chemical innovations that will change our world'.[3] Numerous applications of mechanochemistry have been demonstrated across chemical synthesis,[1,2] crystal engineering,[4] and for the preparation of advanced energy materials.[5] Moreover, mechanochemical technologies are promising for the size-controlled synthesis of catalytically important noble metal nanoparticles (NPs).[6–8] This is an attractive direction for mechanochemical research as traditional solution-phase NP syntheses require severe and solvent-intensive conditions.[9,10]

The mechanochemical synthesis of metal NPs is mostly based on a bottom-up approach. This approach comprises the reduction or decomposition of salt precursors, the generation of the growth species, and their nucleation and growth to produce the final NPs.[11] Qualitative studies have shown how ball milling can generate NPs and nanoclusters.[6–8,12–16] Selective control over NP size and shape, however, remains challenging and poorly understood. In this context, correlations of ball milling parameters with the mechanism of NP nucleation and growth are required. These correlations cannot be established reliably by *ex situ* investigations due to the highly dynamic nature of NP structure during nucleation and growth events.

Recent developments of time-resolved *in situ* techniques for monitoring mechanochemical transformations include powder X-ray diffraction,[17] thermography,[18] vibrational spectroscopy,[19] and manometric approaches.[20] The information attainable by these techniques is, however, limited to molecular and crystalline structure at a bulk level. Established techniques do not provide the information necessary to study precursor reduction, nucleation, and NP growth during bottom-up NP mechanosynthesis. The development of alternative strategies is therefore imperative.

Herein we report a tandem approach for detecting simultaneously the evolution of both electronic and crystalline structure. This time-resolved *in situ* (TRIS) approach comprises two synchrotron-based X-ray techniques: X-ray absorption spectroscopy (XAS) and powder X-ray diffraction (PXRD). We refer to these techniques as TRIS-XAS and TRIS-PXRD, respectively (Fig. 1).

XAS and XRD are complementary techniques. While XRD is sensitive to the long-range bulk order of a material, XAS probes the local environment of the selected absorbing element. In contrast to XRD, XAS does not require large, coherent domains and can therefore monitor developments at significantly smaller length scales.[21,22] The evolution of precursor electronic structure and the initial particle growth stages are therefore captured by XAS. Subsequent growth of particles can be observed through XRD. The combined strength of these techniques has been demonstrated for traditional solution-based NP syntheses.[23,24] Their simultaneous use to follow heterogeneous solid-state reactions represents a significant challenge that has not yet been demonstrated. We develop this strategy for the TRIS monitoring of mechanochemical synthesis, selecting as a model system the formation of technologically

[a] Instituto de Química; Universidade de São Paulo - Av. Lineu Prestes 748, 05508000, São Paulo, Brazil. E-mail: paulofmo@usp.br
[b] Federal Institute for Materials Research and Testing (BAM), Richard-Willstätter-Straße 11, 12489, Berlin, Germany.E-mail: franziska.emmerling@bam.de
[c] Department of Chemistry, University of Helsinki, A.I. Virtasen aukio 1, Helsinki, Finland.
† These authors contribute equally to this work.
Electronic Supplementary Information (ESI) available: Experimental details and complementary characterization. See DOI: 10.1039/x0xx00000x

View Article Online
DOI: 10.1039/D0CC03862H

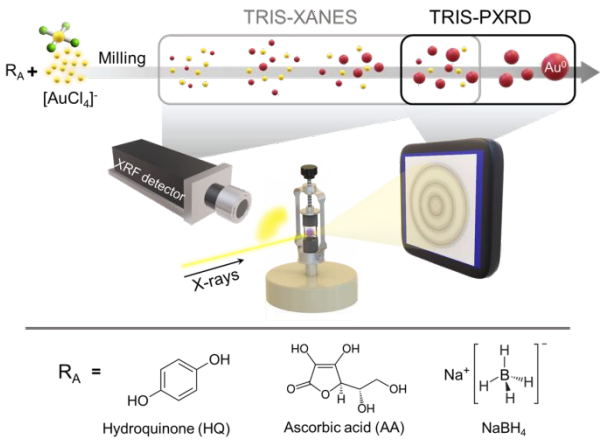


**Fig. 1**. Experimental set up for the time-resolved *in situ* powder XRD (TRIS-PXRD) and XAS (near edge structure; XANES region) (TRIS-XANES) monitoring during mechanochemical synthesis of Au MPs/NPs. The synthesis is based on reduction of $AuCl_4^-$ to $Au^0$ under ball milling conditions using three reducing agents ($R_A$): hydroquinone (HQ), ascorbic acid (AA) and $NaBH_4$. Ball milling was conducted in a vertical vibratory mill (P23, Fritsch) at 50 Hz using custom-made PMMA jars and one $ZrO_2$ milling ball. XRD patterns were collected on an area detector; XANES was acquired in fluorescence mode with a semiconductor detector (XRF detector).

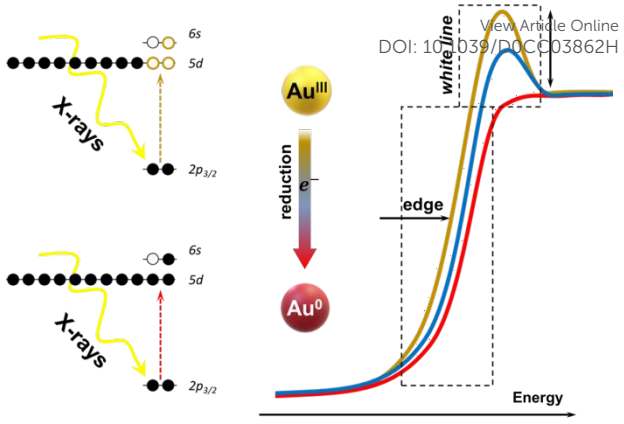


**Fig. 2**. Schematic representation of the physical process underpinning the XANES spectra. X-ray absorption leads predominantly to excitation of a $2p_{3/2}$ electron into a 5d state. The number of available 5d states determines the magnitude of the white line intensity. Hence $Au^{III}$ (yellow in Fig.) will exhibit a strong white line, whereas $Au^0$ (red in Fig.) will not. Dominant XANES features are highlighted in the schematic spectra.

relevant Au MPs/NPs.[25,26] To the best of our knowledge this study represents the first mechanosynthesis monitored simultaneously by combined XRD and XAS.

The mechanochemical synthesis of Au MPs/NPs was carried out with tetrachloroauric acid trihydrate ($HAuCl_4.3H_2O$) as $Au^{III}$ precursor and polyvinylpyrrolidone (PVP) added as a stabilizing agent. Three common reducing agents were used to explore their effect on the transformation: sodium borohydride ($NaBH_4$), ascorbic acid (AA), and hydroquinone (HQ). *Ex situ* transmission electron microscopy (TEM) images show that mechanosynthesis with $NaBH_4$ favours smaller Au NP sizes relative to AA and HQ (ESI Fig.S3), which yield MPs.

Reduction of $Au^{III}$ during the bottom-up synthesis of Au NPs offers an excellent target for XAS-based monitoring. Among XAS methods, X-ray absorption near edge spectroscopy (XANES) is most informative in this context. The XANES region contains critical system-specific information based on (1) the position of the absorption edge, and (2) the intensity of the 'white line' (Fig. 2). These features provide ready characterization of elemental oxidation states as illustrated in Fig. 2. The TRIS-XAS method requires careful selection of the incident X-ray energy, depending on the element of interest. Moreover, care must be taken to minimise absorption of the selected energy by the sample environment (ESI S1.3).

For our system we probe Au at the L-III edge (11,919 eV). Our milling set-up permits sufficient transmission at this energy to allow tandem TRIS-PXRD (ESI Fig S2). $Au^{III}$ absorption at this energy corresponds predominantly to the excitation of core-shell $2p_{3/2}$ to the valence *5d* states.[27] A spectral shift of the absorption edge reflects changes in the Au oxidation state, whereas the white line intensity reflects the number of unoccupied *5d* states. Correspondingly, the time-evolving reduction from $Au^{III}$ to $Au^0$ can be readily followed by monitoring changes in these XANES features (Fig. 2).

The TRIS-XANES obtained for the mechanosynthesis of Au particles displayed similar trends for the different reducing agents, Figs. 3A, C, and E. With an increase in milling time, the absorption edge shifted towards higher energies, accompanied by loss of white line intensity. These spectral features are consistent with reduction of $Au^{III}$ to $Au^0$ during ball milling. The TRIS-PXRD agree with this observation as evidenced by the appearance of Bragg reflections at scattering vectors of q = 26.7 and 30.8 $nm^{-1}$ (Fig. 3-B, D and F). These reflections correspond to the (111) and (200) planes of fcc $Au^0$, respectively.

When considered in isolation, TRIS-PXRD provides an incomplete description of the mechanosynthesis of Au NPs. The highly hygroscopic $HAuCl_4.3H_2O$ is mostly dissolved by atmospheric moisture during manipulation before milling, thereby greatly reducing its crystallinity. Correspondingly, this species remains undetected by our diffraction method. The inability to observe the $Au^{III}$ salt by TRIS-PXRD renders this technique incapable of accurately determining the rate and degree of transformation. Moreover, TRIS-PXRD cannot detect Au clusters or NPs below a critical crystallite size. In contrast, both $Au^{III}$ and $Au^0$ phases are visible by TRIS-XANES, although the presence of non-Au containing phases remains undetected. The complementarity between TRIS-XANES and TRIS-PXRD enables us, in principle, to gather a complete and time-resolved understanding of all stages involved in the mechanosynthesis of metal MPs/NPs.

Further comparison of the time-resolved monitoring of Au particles mechanosynthesis as a function of the reducing agent reveals very promising results for this combination of techniques. During the HQ-based mechanosynthesis, TRIS-XANES (Fig. 3A) suggests the onset of $AuCl_4^-$ reduction begins within the first 15 min of ball milling. The initial rate of $Au^{III}$ reduction is rapid and declines as the reaction progresses. Prolonged milling does not lead to complete reduction of the $AuCl_4^-$ precursor (see Fig. S7). Traces of $Au^{III}$ are still present in the TRIS-XANES spectra after 360 min of ball milling. Owing to the low scattering power of HQ, its low concentration in the powder mixture and the high absorption of X-rays by the

View Article Online
DOI: 10.1039/D0CC03862H

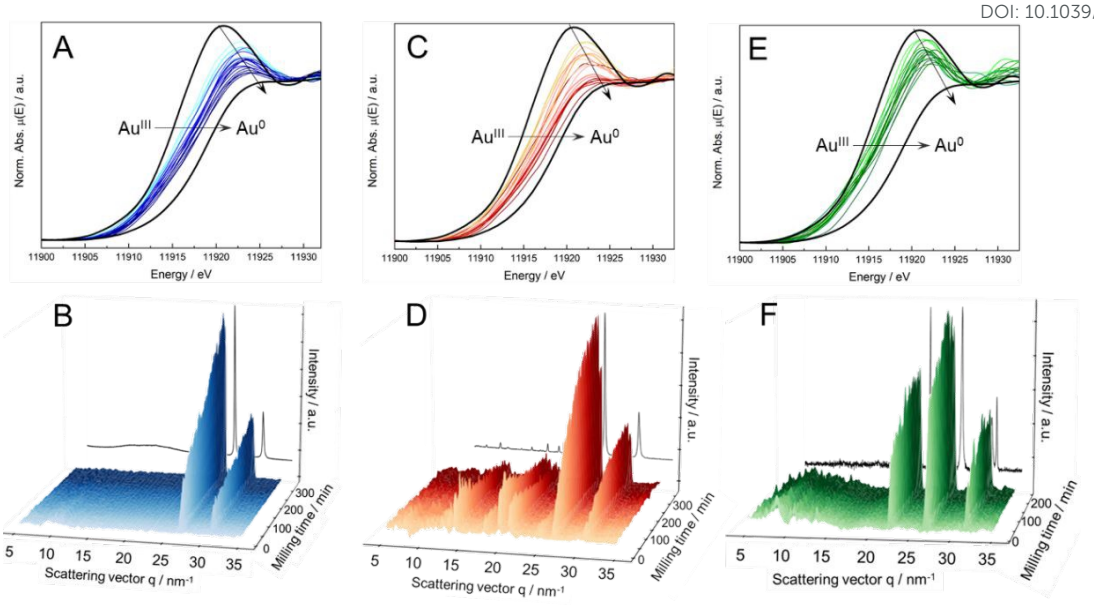


**Fig. 3**. TRIS-XANES (Au-LIII edge) (top) and TRIS-XRD patterns (bottom) for the synthesis of Au NPS under ball milling conditions using hydroquinone (HQ) (A-B), ascorbic acid (AA) (C-D) and NaBH4 (E-F) as reducing agents. The black spectra in A, C and E correspond to the AuIII ($HAuCl_4.3H2O$) and $Au^0$ (foil) standards. The XRD patterns shown as the black traces in B, D, and F are data from ex-situ measurements after the milling period. 2D plots of TRIS-PXRD are also available (Figure S4)

organic media, no traces of HQ or the HQ oxidation product were visible by TRIS-PXRD, Fig. 3B. However, the high intensity of Bragg reflections of the $Au^0$ product phase were readily observed as the reaction progressed.

The rapid onset of $Au^0$ is visible in the TRIS-PXRD patterns within the first 15 min of ball milling, followed by a reduction of the transformation rate with continued milling (Fig. S4). Hence, both TRIS-PXRD and TRIS-XANES support the same kinetics of HQ-driven Au MP formation. This kinetics is consistent with a broad range of mechanochemical transformations.[28] This result suggests that similar factors which underpin organic mechanochemical transformations (e.g. mixing) also dominate the macroscopic dynamics of bottom-up mechanochemical formation of inorganic entities such as metal NPs.[28]

We subsequently consider Au NP mechanosynthesis in the presence of AA. A higher mass fraction of reducing agent was used for the AA-driven reduction of $AuCl_4^-$ as compared with HQ (36% vs 15% by mass; see ESI Table S1). In this case, the reducing agent was also visible by TRIS-PXRD. The first signs of $Au^0$ particle growth were observed by TRIS-PXRD within 15 min of ball milling, as indicated by growth of Bragg reflections at q = 26.7 and 30.8 $nm^{-1}$, Fig. 3D. Moreover, indications of AA consumption were visible within the same frame, as evidenced by a decrease in the Bragg scattering intensities of AA reflections at q = 14.1, 17.9, 19.8, and 21.2 $nm^{-1}$. Both the AA and $Au^0$ PXRD traces suggest that Au particle formation begins very rapidly and slows as the reaction progresses (Fig. S5). This trend is consistent with the HQ-driven mechanosynthesis, albeit more pronounced. The notable AA reflections remaining at the end of the transformation are consistent with the excess AA used in this reaction ($AuCl_4^-$:AA 1:3 molar ratio). No unambiguous information regarding the completeness of the transformation can be gained based on TRIS-PXRD alone. Through our tandem use of TRIS-XANES, Fig. 3C, we observe the onset of the transformation within the first 15 min of ball milling. This is consistent with the TRIS-PXRD data for both AA and $Au^0$. Moreover, the spectroscopic data further support the kinetic trend: very rapid onset (precursor reduction and initial growth), followed by slow progression (growth). In contrast to the HQ-driven reaction, our TRIS-XANES spectra show that AA drives Au particles synthesis to completion over the same milling time (360 min), presumably owing to the excess reagent used. Reaction completion is confirmed by comparison of the final TRIS-XANES spectrum with that of standard $Au^0$ foil (Fig. 3C black curve on the left and Fig. S7).

As a final example, we explore the mechanosynthesis of Au NPs in the presence of $NaBH_4$. In contrast to reduction by AA, $NaBH_4$ is not observed by TRIS-PXRD. In this condition, TRIS-PXRD gave important information on monitoring the rate of product formation. This is because the reduction of $AuCl_4$- by $NaBH_4$ yields highly crystalline NaCl. Within 23 min of ball milling, initial signs of NaCl (Bragg reflections at $q$ = 22.3 and 31.5 $nm^{-1}$) and $Au^0$ (Bragg reflection $q$ = 26.7 $nm^{-1}$) were observed, Fig. 3F. We note that the $Au^0$ reflection at $q$ = 30.8 $nm^{-1}$ which was observed for the other reducing agents, was not detected. This presumably results from the smaller size of Au NPs produced from the reduction with $NaBH_4$ (nm, Fig S1) relative to the synthesis in the presence of AA and HQ ($\mu$m). Monitoring the growth of both NaCl and $Au^0$ Bragg reflections by TRIS-PXRD shows dynamics that are consistent with both AA and HQ: rapid reaction onset, followed by a gradual decrease in reaction rate (Fig. S4). Hence, we suggest this kinetic profile is general, does not strongly depend on the reducing agent, and

can be applied to describe the mechanochemical synthesis of Au NPs.

Remarkably, our tandem TRIS-XANES spectra indicate that the $NaBH_4$-driven Au reduction begins within only 15 min of milling – i.e. consistent with the onset times observed by both HQ and AA. The discrepancy between TRIS-XANES and -PXRD presumably results from the smaller sizes of $NaBH_4$-driven NPs, which make them difficult to detect by diffraction methods before they grow past a critical size. Overall, the kinetic trends observed by TRIS-XANES are consistent with the PXRD data and offer additional insight regarding the extent of the reaction. After 240 min of milling when the reaction was stopped, a comparison of the final TRIS-XANES with standard $Au^0$ foil suggests a mixture of both $Au^0$ and $Au^{III}$ (Fig. S7). Despite $NaBH_4$ being present in large molar excess (Table S1), it was not able to drive the reaction to completion. $NaBH_4$ is a strong reducing agent in solution; however, the present results suggest a significantly different behaviour under mechanochemical conditions.

In summary, we report a new tandem approach to simultaneously monitor the evolution of electronic and crystal structure during the mechanochemical synthesis of Au MPs/NPs. This was achieved by combining two complementary synchrotron-based techniques: X-ray absorption spectroscopy and X-ray diffraction. The tandem configuration and complementary provided *in situ*, time resolved insight into precursor reduction, generation of $Au^0$ species (related to nucleation), and Au NP growth. More specifically, X-ray diffraction revealed the time-dependent evolution of crystalline materials, including the consumption of reducing agents and formation of by-products. These species are invisible to the spectroscopic method, which is specific to our selected element: Au. Instead, X-ray absorption provided unique insights into the extent of Au reduction (i.e. changes in the electronic structure). Moreover, the spectroscopic approach enhances the overall sensitivity of our experiments, allowing us to identify transformations below the sensitivity of X-ray diffraction. Our data indicate that the mechanosynthesis of Au MPs/NPs follow a general kinetics profile which is well-established across a broad range of mechanochemical reactions. By varying the incident X-ray energy our approach can be applied to study a plethora of mechanosyntheses, including NPs of other noble and non-noble metals. We expect this approach to become a key tool in the mechanochemistry toolbox and help pave the way to rationally design nanomaterials with targeted sizes, shapes, compositions, and functionalities.

Experiments were conducted at µSpot (BESSY-II; Helmholtz-Zentrum Berlin). Dr I. Zizak and Ms. Röder are thanked for technical assistance, and Mr. C. Prinz for TEM images. PFMO thanks Sao Paulo Research Foundation FAPESP for fellowships (FAPESP 2019/01619-0 and 2017/15456-0). R.M.T. thanks CNPq, CAPES and FAPESP (2015/26308-7) for financial support. P.H.C.C. thanks Jane and Aatos Erkko foundation and University of Helsinki for financial support.

## Conflicts of interest

There are no conflicts to declare.

View Article Online
DOI: 10.1039/D0CC03862H

## Notes and references

1 E. Boldyreva, *Chem. Soc. Rev.*, 2013, **42**, 7719.
2 T. Friščić, C. Mottillo and H. M. Titi, *Angew. Chemie Int. Ed.*, 2020, **59**, 1018–1029.
3 F. Gomollón-Bel, *Chem. Int.*, 2019, **41**, 12–17.
4 D. Braga, L. Maini and F. Grepioni, *Chem. Soc. Rev.*, 2013, **42**, 7638.
5 M. J. Muñoz-Batista, D. Rodriguez-Padron, A. R. Puente-Santiago and R. Luque, *ACS Sustain. Chem. Eng.*, 2018, **6**, 9530–9544.
6 P. F. M. de Oliveira, J. Quiroz, D. C. de Oliveira and P. H. C. Camargo, *Chem. Commun.*, 2019, **55**, 14267–14270.
7 M. J. Rak, N. K. Saadé, T. Friščić and A. Moores, *Green Chem.*, 2014, **16**, 86–89.
8 D. Debnath, S. H. Kim and K. E. Geckeler, *J. Mater. Chem.*, 2009, **19**, 8810–8816.
9 J. Turkevich, P. C. Stevenson and J. Hillier, *Discuss. Faraday Soc.*, 1951, **11**, 55.
10 F. Fievet, J. P. Lagier and M. Figlarz, *MRS Bull.*, 1989, **14**, 29–34.
11 A. Moores, *Curr. Opin. Green Sustain. Chem.*, 2018, **12**, 33–37.
12 T. U. B. Rao, B. Nataraju and T. Pradeep, *J. Am. Chem. Soc.*, 2010, **132**, 16304–16307.
13 D. Debnath, C. Kim, S. H. Kim and K. E. Geckeler, *Macromol. Rapid Commun.*, 2010, **31**, 549–553.
14 T. Premkumar and K. E. Geckeler, *Colloids Surfaces A Physicochem. Eng. Asp.*, 2014, **456**, 49–54.
15 B. Bokhonov, I. Konstanchuk, E. Ivanov and V. Boldyrev, *J. Alloys Compd.*, 1992, **187**, 207–214.
16 T. Tsuzuki and P. G. McCormick, *J. Mater. Sci.*, 2004, **39**, 5143–5146.
17 T. Friščić, I. Halasz, P. J. Beldon, A. M. Belenguer, F. Adams, S. a J. Kimber, V. Honkimäki and R. E. Dinnebier, *Nat. Chem.*, 2013, **5**, 66–73.
18 H. Kulla, S. Haferkamp, I. Akhmetova, M. Röllig, C. Maierhofer, K. Rademann and F. Emmerling, *Angew. Chemie Int. Ed.*, 2018, **57**, 5930–5933.
19 L. Batzdorf, F. Fischer, M. Wilke, K.-J. Wenzel and F. Emmerling, *Angew. Chemie Int. Ed.*, 2015, **54**, 1799–1802.
20 S. Doppiu, L. Schultz and O. Gutfleisch, *J. Alloys Compd.*, 2007, **427**, 204–208.
21 A. I. Frenkel, Q. Wang, N. Marinkovic, J. G. Chen, L. Barrio, R. Si, A. L. Cámara, A. M. Estrella, J. A. Rodriguez and J. C. Hanson, *J. Phys. Chem. C*, 2011, **115**, 17884–17890.
22 S. N. Ehrlich, J. C. Hanson, A. Lopez Camara, L. Barrio, M. Estrella, G. Zhou, R. Si, S. Khalid and Q. Wang, *Nucl. Instrum. Methods Phys. Res., Sect. A*, 2011, **649**, 213–215.
23 J. Polte, R. Erler, A. F. Thünemann, S. Sokolov, T. T. Ahner, K. Rademann, F. Emmerling and R. Kraehnert, *ACS Nano*, 2010, **4**, 1076–1082.
24 M. Staniuk, O. Hirsch, N. Kränzlin, R. Böhlen, W. Van Beek, P. M. Abdala and D. Koziej, *Chem. Mater.*, 2014, **26**, 2086–2094.
25 X. Yang, M. Yang, B. Pang, M. Vara and Y. Xia, *Chem. Rev.*, 2015, **115**, 10410–10488.
26 M. Stratakis and H. Garcia, *Chem. Rev.*, 2012, **112**, 4469–4506.
27 J. Ohyama, K. Teramura, T. Shishido, Y. Hitomi, K. Kato, H. Tanida, T. Uruga and T. Tanaka, *Chem. Phys. Lett.*, 2011, **507**, 105–110.
28 A. A. L. Michalchuk, I. A. Tumanov, S. Konar, S. A. J. Kimber, C. R. Pulham and E. V. Boldyreva, *Adv. Sci.*, 2017, **4**, 1700132.

View Article Online
DOI: 10.1039/D0CC03862H

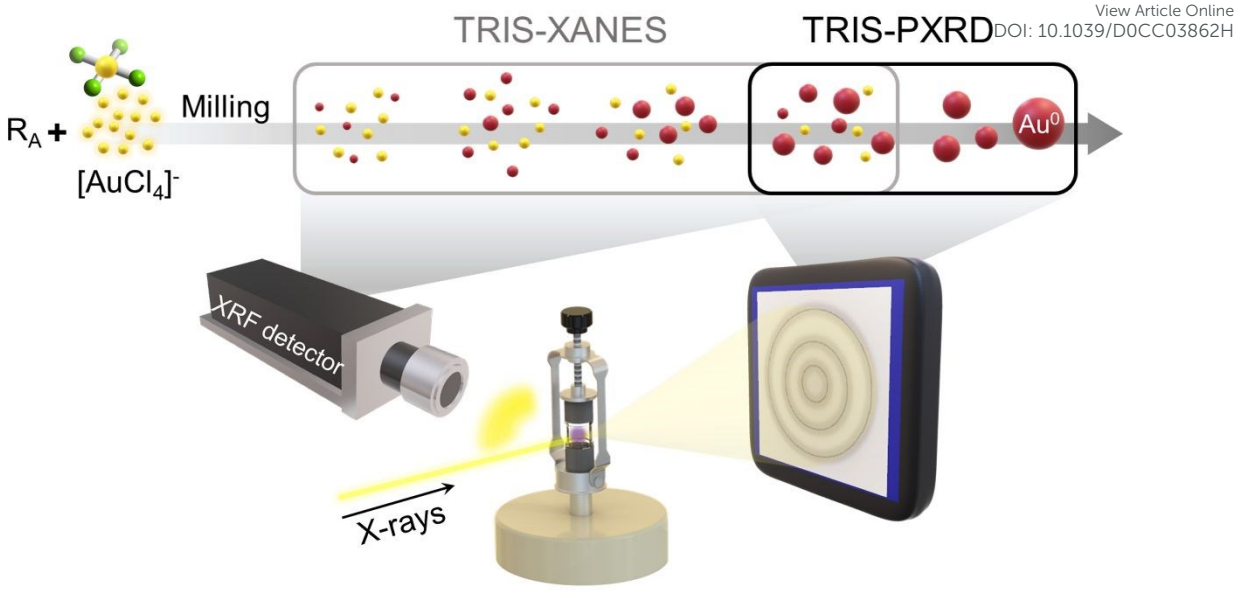


A new tandem approach combines XRD and XANES for time-resolved *in situ* monitoring the mechanochemical synthesis of gold nanoparticles.